Acidic medium synthesis of zeolites – an avenue to control the structure-directing power of organic templates

Guangying Fu, Eddy Dib, Qiaolin Lang, Haonuan Zhao, Songxia Wang, Ruiqin Ding, Xiaobo Yang, Valentin Valtchev

ARTICLE

Acidic medium synthesis of zeolites – an avenue to control the structure-directing power of the organic template

Received 00th January 20xx,
Accepted 00th January 20xx

DOI: 10.1039/x0xx00000x

Guangying Fu,[a] Eddy Dib,[b] Qiaolin Lang,[a] Haonuan Zhao,[a,b] Songxia Wang,[a] Ruiqin Ding,[a] Xiaobo Yang,*[a] and Valentin Valtchev*[a,b]

This paper deals with the extension of the synthesis field of microporous zeolite-type materials and the type of organic structure-directing agents (OSDA) that can be used to promote their crystallization. The highly hydrophilic hexamethylenetetramine (urotropine), with its C/N ratio = 1.5 , which is unusual to act as a structure-directing agent in the crystallization of open-framework silica polymorphs, is used to exemplify the novelty of the employed approach. Namely, the protonation of urotropine in an acidic fluorine-containing medium transforms it into a very efficient OSDA that yields dodecasil 3C (**MTN**-type). This novel synthesis also allows getting insights into OSDA-framework interactions in the **MTN**-type structure. The comprehensive ^{29}Si and ^{19}F MAS NMR indicate a small number of point defects of the framework T sites and the multiple bonding of F^- ions to Si in a disordered manner. Based on this finding, a unit cell model has been generated using Monte Carlo simulation and validated with Rietveld refinement using experimental powder X-Ray diffraction data. In the model, protonated urotropine cations are located in the center of the big hexakaidecahedral [$5^{12}6^4$] cages at full occupancy with random orientations. The charge balance is provided by the disordered F^- ions.

1 Introduction

The structure-directing role of an organic compound in the synthesis of microporous crystalline tectosilicates is an intensively investigated yet far from fully clarified research topic.[1-9] In the synthesis of high-silica zeolites, the organic structure-directing agent (OSDA) is a very important element in determining the crystalline phase of the product, i.e., the framework topology and the phase purity, by organizing the inorganic zeolitic structural units and driving the crystallization pathways towards a particular framework topology.[2] The OSDA, with the characteristics such as appropriate size and shape, justified rigidity/flexibility, as well as balanced hydrophobicity/ hydrophilicity, interacts with silicate species in the liquid phase of the initial hydrogel to generate the first nuclei. In a later stage, OSDA interacts with the growing crystal surfaces until the crystallization process completes. While multiple factors such as the presence of a mineralizer, the water content in the initial gel composition, and the conditional parameters of hydrothermal treatment (temperature, pressure, and duration), contribute to the product phase selection at various degrees, the role of OSDA among them is recognized as decisive.[5, 10]

Taking **MFI**-type zeolite as a representative example, Davis et al. illustrated [11, 12] that zeolite formation is initiated by the reaction between the structure-directing agent, usually a cation or positively charged molecule, and silicate anions in the zone of supersaturation. Silicate anions approach the OSDA cation, substitute water molecules in the cation's hydrate shield, and become hydrolyzed/condensed with each other. Thus, an organized structure of OSDA/oligomerized silicates is formed. These structured composites assemble themselves further to form nuclei, which ignite the process of crystal growth after reaching a critical size. The interface of gel particles to the solution phase is considered the place where the fast exchange between liquid and solid phases facilitates nuclei formation.[13-15]

The size, shape, and rigidity/flexibility of OSDA may have the main impacts on the organic/inorganic composite structure that is later translated to the size and shape of the framework cages and channels.[16] The hydrophobicity/hydrophilicity of the OSDA may be taken as a measure of the interaction strength between OSDA and the oxo-anionic framework building-blocks. The strength of interaction determines whether the structured composite can form, how stable it is, and how the energetics is when it grows. For amine and ammonium OSDAs, Zones et al. put forward a rule-of-thumb that those organic species with C/N ratios between 10-16 possess balanced hydrophobicity/ hydrophilicity that provide the proper strengths of organic/inorganic interactions.[17] Most of the

[a] *The ZeoMat Group, Qingdao Institute of Bioenergy and Bioprocess Technology, CAS, Laoshan District, CN-266101 Qingdao, China. e-amil: yangxb@qibebt.ac.cn.*
[b] *Normandie University, ENSICAEN, UNICAEN, CNRS, Laboratoire Catalyse et Spectrochimie, F-14000 Caen, France. e-mail: valentin.valtchev@ensicaen.fr.*

† Electronic Supplementary Information (ESI) available: Additional synthetic and characterization results; Molecular simulation results; Rietveld refinement conditions and results; .cif files and .msi models. See DOI: 10.1039/x0xx00000x

known OSDAs for zeolite synthesis are found within this window.

In this work, we introduce an OSDA out of this rule, i.e., hexamethylene-tetramine (HMTA, or urotropine). Urotropine molecule has the same shape as adamantane, but with four N atoms at the vertexes of cycles instead of C atoms. A vast number of amines and organic ammonium ions of similar cyclic and polycyclic shapes were tested as OSDAs in the synthesis of clathrasils and zeolites.[1, 18-20] However, urotropine has been overlooked, probably due to the low C/N ratio and thus its high hydrophilicity, which would usually establish a strong interaction with its hydrate shield in an aqueous medium, preventing the necessary interaction with silicates.[2, 16, 17] We have employed urotropine to verify our hypothesis that changing the synthesis medium from basic to acidic might alter the structure-directing ability of an organic molecule in zeolite synthesis.

Recently we have demonstrated that the chemistry field for the hydrothermal crystallizations of silicalite-1[21, 22] and some other zeolite-type tectosilicate materials[23] can be extended from the conventional basic and near-neutral conditions to the strongly acidic region. Besides elaborating on the unique structural and surface-chemical properties of the zeolite products obtained in the acidic media, we have also predicted the possibility of discovering new OSDAs that do not work under the basic conditions but become feasible in the extended chemistry field.

The present study uses urotropine that does not show any structure-directing properties in the synthesis of zeolites in the basic medium. Thanks to the protonation in an acidic HF-containing medium, $HMTA^+$ yielded a microporous clathrasil with the **MTN** framework topology. ^{29}Si MAS NMR and ^{19}F MAS NMR measurement of the acidic medium product reveal the existence of framework T defects and the bonding of multiple F^- ions to framework Si. Based on the experimental observations, we carry out an energy minimization simulation using the Monte Carlo protocol to locate the occluded $HMTA^+$. The simulated model has been validated against experimental XRD by Rietveld refinement. The Rietveld refinement confirms the location and orientation of $HMTA^+$ ions, and explains that $HMTA^+$ has a strong structure-directing power because it fits perfectly into **MTN**'s [$5^{12}6^4$] cage.

2 Experimental

2.1 Hydrothermal synthesis

Materials. Hexamethylene-tetramine (HMTA, urotropine, P.A. Sinopharm), tetramethylammonium hydroxide (TMAOH, 25 wt.% aq., Sinopharm), hydrobromic acid (HBr, 40 wt.% aq., Aladine), hydrofluoric acid (HF, 40 wt.% aq., Macklin), colloidal silica (30 wt.% suspension in H_2O, SiO_2/NaOH = 100, Macklin), were used as purchased without further purification. Deionized (DI) water was used throughout the synthetic experiments.

Synthesis. Table 1 summarizes the synthetic experiments with respective gel compositions and hydrothermal conditions. For each experiment, 0.7 g HMTA was dissolved in the proper amount of H_2O. Then 2.0 g colloidal silica (30 wt.%) was added dropwise under stirring. The mixture was stirred further for 24 hours at room temperature. Then calculated amounts of NH_4F/HF/HBr (aq.) according to the targeted compositions were added, and the gel was stirred for another 30 minutes. The pH of the homogenized gel was recorded with a pH meter. The gel was sealed in a Teflon-lined autoclave. The crystallizations were performed statically at 140°C-180°C for 21-39 days. The recovered solid products were washed three times with water and dried at 80°C in air.

A reference material (R1 in Table 1, $|TMA^+,F^-|$-dodecasil 3C-**MTN**) was synthesized from a basic gel of the composition $1SiO_2$: 1.1TMAOH: $1.8NH_4F$: $40H_2O$, at 180°C in 14 days according to the recipe adapted from the literature.[24]

2.2 Characterization

Powder X-ray diffraction was performed at room temperature on a RIGAKU SmartLab Diffractometer. The diffractometer uses Cu Kα radiation (λ = 1.5418 Å, 40 kV, 150 mA), and works in the theta-theta geometry. Samples were pressed on a glass plate. Continuous scans with an 1D detector at a scanning speed of 20.00°/min at 0.01° steps were used for phase identifications. The as-synthesized powders were used directly

Table 1. The gel compositions, hydrothermal synthesis conditions and the products obtained in present study.

Exp#	Gel molar composition	pH	T(°C)	t(days)	Product
A1	$1SiO_2$:0.5HMTA:$50H_2O$	9.5	160	21	No crystallization
A2	$1SiO_2$:0.5HMTA:$0.056NH_4F$:0.083HF:$20H_2O$	6.8	160	21	**MTN**
A3	$1SiO_2$:0.5HMTA:$0.056NH_4F$:0.083HF:$50H_2O$	6.1	160	21	**MTN**
A4	$1SiO_2$:0.5HMTA:0.125HF:$50H_2O$	5.8	160	31	**MTN**
A5	$1SiO_2$:0.5HMTA:0.125HF:0.04HBr:$50H_2O$	5.6	160	31	**MTN**
A6	$1SiO_2$:0.5HMTA:0.125HF:0.2HBr:$20H_2O$	4.4	160	39	**MTN**
B7	$1SiO_2$:0.5HMTA:0.125HF:$80H_2O$	5.5	160	30	**MTN**
B8	$1SiO_2$:0.5HMTA:0.125HF:$20H_2O$	5.9	160	30	**MTN**
B9	$1SiO_2$:0.5HMTA:0.125HF:$8H_2O$	6.2	160	30	**MTN**
C10	$1SiO_2$:0.5HMTA:$0.056NH_4F$:0.083HF:$50H_2O$	6.5	180	36	Cristobalite
C11	$1SiO_2$:0.5HMTA:0.125HF:$50H_2O$	5.6	140	39	Amorphous
R1	$1SiO_2$:1.1TMAOH:$1.8NH_4F$:$40H_2O$	12.8	180	14	**MTN**

to prepare the samples without grinding to emphasize the preferred orientations that may arise due to non-random alignments of big crystals with certain shapes. A slow step-scan using a 0D detector at a speed of 3 s/0.01° was performed for structural analysis of a selected sample (A3 in Table 1). For this purpose, the powder was thoroughly ground and carefully pressed onto the sample holder to eliminate a preferred orientation.

Scanning Electron Microscopy (SEM) images of the samples were recorded on a JEOL JSM-6700F Microscope, which was equipped with a cold field emission gun operated at 1~2 kV.

^{29}Si MAS NMR experiments were performed on Bruker AVANCE III 600 spectrometer at a resonance frequency of 119.2 MHz. ^{29}Si MAS NMR spectra with high-power proton decoupling were recorded on a 4 mm probe with a spinning rate of 10 kHz, a π/4 pulse length of 2.6 µs, and a recycle delay of 60 s. The chemical shifts of ^{29}Si are referenced to TMS.

^{19}F MAS NMR was carried out on a Bruker AVANCE III 600 spectrometer at a resonance frequency of 564.5 MHz using a 4 mm HX double-resonance MAS probe at a sample spinning rate of 15 kHz. ^{19}F MAS NMR spectra were recorded with a π/2 pulse length of 3.5 µs and a 10 s recycle delay. The chemical shifts were referenced to $CFCl_3$ at 0 ppm.

TG/DTA analysis was performed using Rigaku TG-DTA8122 microbalance upon ca. 10 mg zeolite powder against α-Al_2O_3, in 50 ml/min reconstituted (80% N_2 + 20% O_2) airflow at a heating rate of 10°C/min in the temperature range from room temperature to 1300°C.

2.3 Molecular simulations combined with experimental XRD

In the structure database of the International Zeolite Association, **MTN** topology is given as a framework of SiO_2 in the cubic unit cell Fd-3m (#227) of a = 19.9330(0) Å.[25] Le Bail fitting[26] of the experimental XRD of sample A3 gives a unit cell parameter a = 19.392188(289) Å, with zero offset -0.015(2)°. We used the experimental unit cell parameter to create a P1 cell of the framework in the pcff force field using the Sorption module of Materials Studio. $5 \cdot 10^6$ configurations of $HMTA^+$ were generated by the Monte Carlo method Metropolis. Energy minimization was performed at 298 K and 101.3 kPa, in order to verify the loading of $HMTA^+$ at this condition.[27] A simulated annealing was performed[28] using the adsorption Locator module of Materials Studio, and a P1 model of $|HMTA^+_8|[Si_{136}O_{272}]$ was obtained. Then the model was validated against experimental XRD using GSAS II[29] by a Rietveld full pattern fitting.[30] The experimental profile parameters and the unit cell parameters were refined. The atomic coordinates were kept unchanged as in the simulated model, in order to avoid random relaxations. The refinement conditions are given in Table 2. The resulting atom list, and the Crystallographic Information File are provided in the Supplementary Information.

3 Results and discussion

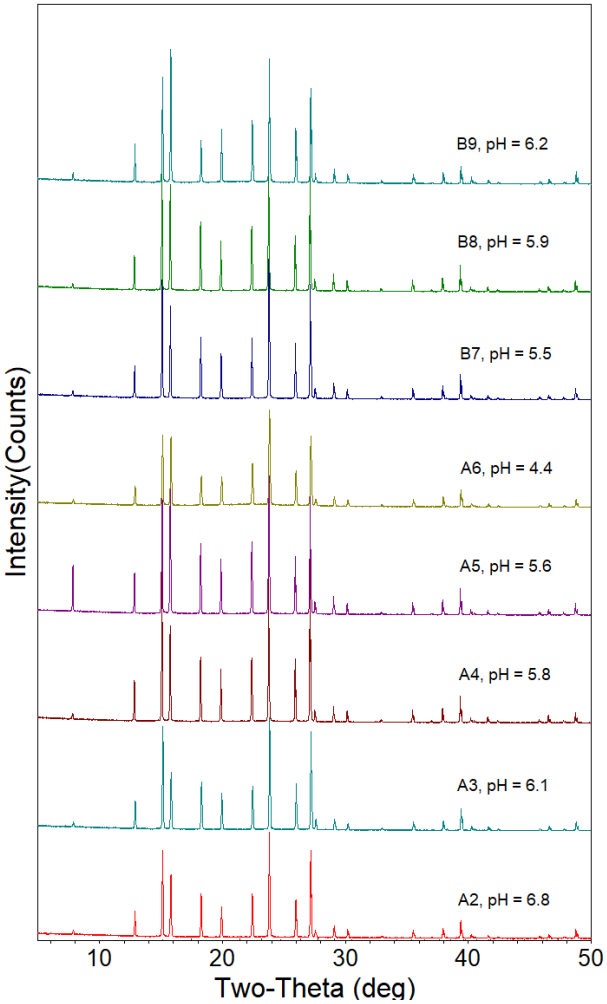

Figure 1. XRD patterns of the solid products throughout experiments A2 to B9. The investigation A1 did not crystallize. From A2 to B9 are crystals of the pure **MTN** phase obtained at various conditions according to Table 1. The XRD patterns of C10 (cristobalite) and C11 (amorphous) are shown in Figure S2 in the Supplementary Information.

3.1 |$HMTA^+$, F^-|-[SiO_2]-dodecasil 3C-MTN crystallizes at pH = 4.4 ~ 6.8

Dodecasil 3C-**MTN**,[31] and the aluminosilicate version ZSM-39 with Si/Al = 100 - ∞,[32] have been synthesized previously using tetramethylammonium (TMA^+), tetraethylammonium (TEA^+), 1-aminoadamantane, and a number of other organic amines as OSDA in basic conditions.[33-35] Using TMA^+ as OSDA, the crystallization of **MTN** occurred in a fluoride medium as well.[24] **MTN** framework is isostructural to the 17 Å cubic clathrate gas hydrate (Type II), which contains two kinds of cages: the hexakaidecahedral [$5^{12}6^4$] cage, and dodecahedral [5^{12}] cage.[36] Table 1 shows the robustness and selectivity of HMTA as OSDA for dodecasil 3C in an acidic medium in a broad range of water content (H_2O/SiO_2 = 8-80) and a pH range varying between 4.4 and 6.8. The situation with the strong affinity of the molecule to water and the insufficient interactions with silicate species, which is not suitable for zeolite crystallization, is changed in the chosen conditions.

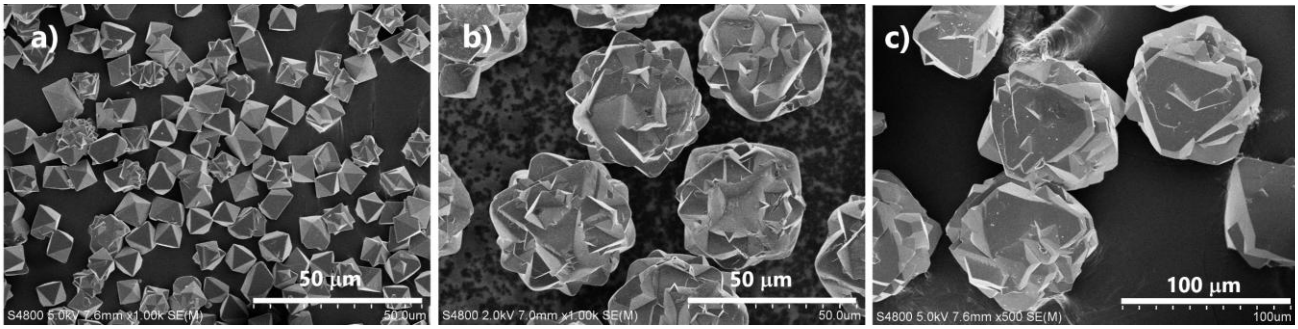

Figure 2. SEM pictures of dodecasil 3C-**MTN** crystallized from hydrogels of a) pH= 6.1 (Sample A3), b) pH =5.6 (Sample A5), and c) pH = 4.4 (Sample A6).

The series A experiments were designed to investigate the pH dependence of the crystalline phase selection. The hydrogel $1SiO_2$: 0.5HMTA: $50H_2O$ without an additional acid had a pH value of 9.5. It remained a soft and translucent gel and did not crystallize at 160°C in 21 days. The pH of the gel was basic, where HMTA did not become protonated.

Then the pH values of the gels were decreased to 6.8-4.4 gradually by adding appropriate amounts of NH_4F/HF/HBr solutions with increasing acid contents, while the amount of F^- ions was kept constant. These pH values correspond to the range below the pK_a of HMTA, giving rise to protonated monovalent cation, $HMTA^+$. In literature, $pK_{a,1}$ values of HMTA for the protonation of a first N atom out of the 4 equivalents in solutions of various acids with different concentrations ranging from 8.85,[37] 5.18,[38] to 4.89.[39] The $pK_{a,2}$ for the protonation of a second N atom to form $HMTA^{2+}$ cation is below 2.0.[39] In the present experimental pH range mainly $HMTA^+$ is present, and pure **MTN** crystals were obtained. The crystallization time extended from 21 days to 39 days with descending pH values (Figure 1). The ratio of F^-/SiO_2 was kept at 0.125 in these experiments. Higher F^-/SiO_2 ratios require a longer time for crystallization. For example, for a gel of the composition $1SiO_2$: 0.5HMTA: $0.12NH_4F$: 0.18HF: $50H_2O$ and pH = 5.9, 30 days are needed for **MTN** crystals to appear, but a certain amount of the gel still remained amorphous (Figure S1.1 in Supplementary Information). The slow crystallization is due to the high solubility of SiF_6^{2-}, preventing the rapid establishment of supersaturation.

The variations of H_2O content in the initial gels in experiment series A between 20 and 50 show that **MTN** crystallization was not sensitive to H_2O content in these recipes. The experiment series B was to confirm this point. The gels with H_2O/SiO_2 = 8-80 at pH around 6 was subjected to the hydrothermal condition at 160°C for 30 days. All batches yielded **MTN**.

Temperature variation was studied in the C series of experiments. At 180°C, HMTA decomposed, and cristobalite was produced in 30 days. The crystallization of the dense phase of silica does not require an OSDA. The lower temperature did not lead to **MTN** crystals as well. The crystallization at 140°C was too slow, and separation of an aqueous solution phase and a shrunken gel phase was just observable after 39 days. The recovered and dried solid was amorphous (Figure S1.2 in Supplementary Information).

Figure 1 shows the XRD of all recovered solid products from experiments A2 to B9. Based on the peak positions, they are all pure **MTN** phases. The differences in the relative peak intensities, i.e., different preferred orientations under the XRD measurements, are the consequence that the crystals have different shapes and big size. As one example among many, the Sample A5 exhibits an unusually high intensity of the (111) peak at $2\theta = 2.89°$, corresponding to an abnormal exposure of this plane parallel to the sample surface when the powder of big and intergrown crystals was pressed to the sample plate without grinding.

Reprehensive SEM images of three samples crystallized at different pH values are shown in Figure 2. The product obtained at pH = 6.1 in 21 days (Sample A3) are octahedral crystals, and occasionally intergrown particles of octahedra of about the same sizes, with ca. 10 μm edge length. Larger, ca. 40 μm, agglomerate of intergrown octahedral crystals, were obtained for 31 days from a gel with pH = 5.6. Similar morphology but with larger aglomerates (ca. 80 μm) of larger individual crystals was obtained from the gel with pH = 4.4 after 39 days of crystallization. Thus, the product grows bigger with decreasing pH in the initial gel and increasing time for crystallization.

These synthetic experiments show that urotropine in its molecular form indeed does not act as an OSDA under the tested conditions. Only when it becomes protonated to $HMTA^+$, the cation interacts stronger with silicate species, therewith, the exchange of water and silicates in the hydrate shield of $HMTA^+$ is enabled. Under the tested conditions, $HMTA^+$ promotes the crystallization of **MNT**-type material in a broad range of concentrations at pH = 4.4-6.8. The protonation to the monovalent cation endows urotropine the power of OSDA.

3.2 The multiple bonding of F^- to framework Si

In ^{29}Si MAS NMR spectra of dodecasil 3C-**MTN** samples obtained at pH = 6.1 and 4.4 (Figure 3), there are three Q^4 ($Si(OSi)_4$) peaks at -101.2, -115.9, and -118.9 ppm with area ratios of 1/6/10, respectively. Comparing the three distinctive T sites in the

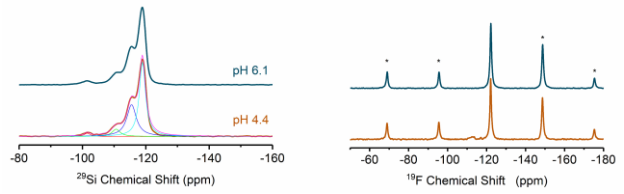

Figure 3. ^{29}Si MAS NMR and ^{19}F MAS NMR of |HMTA$^+$,F$^-$|-dodecasil 3C-**MTN** crystallized from hydrogels of pH= 6.1 and 4.4 (Sample A3 and A6).

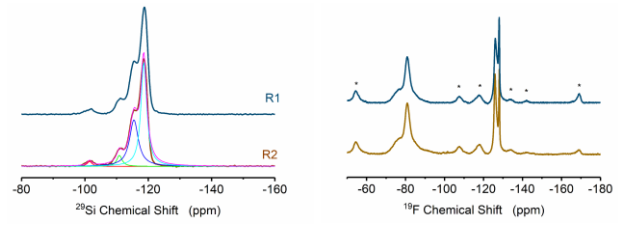

Figure 4. ^{29}Si MAS NMR and ^{19}F MAS NMR of |TMA$^+$, F$^-$|-dodecasil 3C-**MTN** crystallized from a basic hydrogel, Sample R1 and its re-production R2.

Fd-3m unit cell: T1 has a site symmetry of m(±0), therefore a multiplicity of 96; T2 has a site symmetry 3m(111) and multiplicity of 32; T3 has -43m and a multiplicity of 8. Thus, the Q^4 peaks are, in turn, assigned to T3, T1/T2, and T1.[40-42]

However, ^{29}Si MAS NMR shows an additional peak at -101.2 ppm, which is in the region of Q^3 (X-Si-(OSi)$_3$), with a peak area of ca. 2% of total Si peaks. It is abnormal to have a significant Q^3 signal for a zeolitic material that has been slowly crystallized in a fluoride medium because those materials are expected to be free of point defects.[1, 43-45] The amount of Q^3 of both samples is similar, i.e., point defects in the framework T atoms repeatedly occur at different pH, although their concentration is low, and the frameworks are still highly ordered.

Furthermore, F$^-$ anions that reside in crystalline voids and bond weakly to framework Si sites usually stimulate a broad so-called Q^5 (F–Si-(OSi)$_4$) peak in ^{29}Si MAS NMR, a peak that is not observed in the current spectra. Such species are usually observed with ^{19}F NMR in a chemical shift range between -50 and -80 ppm.[46, 47]

^{19}F MAS NMR spectra present a spinning sideband pattern with an isotropic central band at -122.1 ppm (Figure 3). The deconvolution of the corresponding spectra being impossible with a unique site characterized by a precise set of parameters for the chemical shift anisotropy, it is plausible to attribute the observed -122.1 ppm ^{19}F NMR peaks to multiple environments of F$^-$ anions connected with framework Si sites *i.e.,* F$_x$–Si(-OSi)$_3$ with x > 1, noting the large width of the spinning sideband pattern. In other words, multiple environments of F$^-$ anions bond strongly to Si sites present in the framework and show restricted mobility. It should be noted that the F$^-$ in SiF_4 has a chemical shift δ(^{19}F) of -162 ppm,[48] while SiF_6^{2-}, which is often present in the hydrogels for zeolite crystallization, shows a chemical shift δ(^{19}F) of -123 to -128 ppm.[47]

A reference material |TMA$^+$, F$^-$|-dodecasil-3C-**MTN** has been synthesized with TMAOH as OSDA in a basic medium. The purity of the crystalline phase is illustrated by XRD in Figure S1.3. And the SEM image (Figure S1.4) shows big octahedral crystals with edge lengths around 180 µm. Figure 4 shows the corresponding ^{29}Si and ^{19}F MAS NMR spectra, around 2% of Q^3 species are also present in this material, however, F$^-$ ions experience also the highly disordered environments despite the presence of a small fraction entrapped in the [5^{12}] cages with δ(^{19}F) of -80.9 ppm.

3.3 The location of HMTA$^+$ in |HMTA$^+$,F$^-$|[Si$_{136}$O$_{272}$]-dodecasil 3C-MTN

The energy minimization at 298 K and 101.3 kPa reveals loadings of 8 HMTA$^+$ ions in a unit cell with a = 19.392188 Å (value from Le Bail fitting). Out of $5{\cdot}10^6$ Monte Carlo configurations, settled HMTA$^+$ ions populate at the centers of the hexakaidecahedral [$5^{12}6^4$] cage, with full occupancy (Figure S2.1, and corresponding 3D model as HMTA+population.msi). The isosteric heat of adsorption is 81.3 kcal/mol, which is a high value corresponding to a strong interaction between HMTA$^+$ and the cage walls.

The model of the P1 cell with settled HMTA$^+$ ions, as a result of the simulated annealing, is illustrated in Figure 5. The corresponding 3D model is provided in the Supplementary Information as HMTA+Orientations.msi.

HMTA$^+$ is nearly spherical. The cation is located in the center of **MTN**'s [$5^{12}6^4$] cage. There are no short contacts between the guest atoms and the framework atoms. Random molecular orientations are obtained. This explains the random distribution of F$^-$ ions and point defects in the siliceous framework considering the charge balance and the multiple F$^-$ ion environments in addition to the existence of point defects. Without siloxy defects, 8 F$^-$ ions are required to balance the positive charges of 8 HMTA$^+$ cations. XRF analyses of sample A3 and A6 have shown fluorine contents around 0.75 wt.% in both materials, corresponding to ca. 4 F$^-$ in a unit cell. If we tolerate the measurement error of XRF method, additional point defects are required for charge balancing, in line with the ^{29}Si NMR spectra showing 2% of Q^3 species. Therefore, the unit cell has an approximate formula |HMTA$^+_8$,F$^-_{\sim 4}$|[Si$_{136\cdot(1\text{-}2\%)}O_{272}$]-dodecasil 3C-**MTN**.

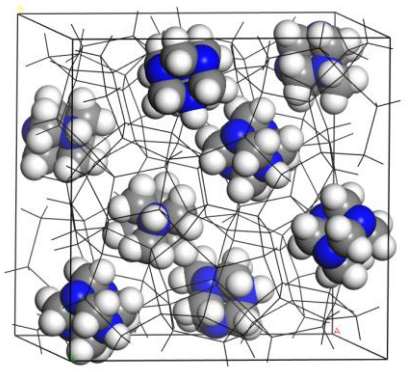

Figure 5. The simulated annealing process reveals that HMTA$^+$ cations are located at the centers of the hexakaidecahedral [$5^{12}6^4$] cages with random orientations, at the full occupancy, i.e., 8 cations per unit cell.

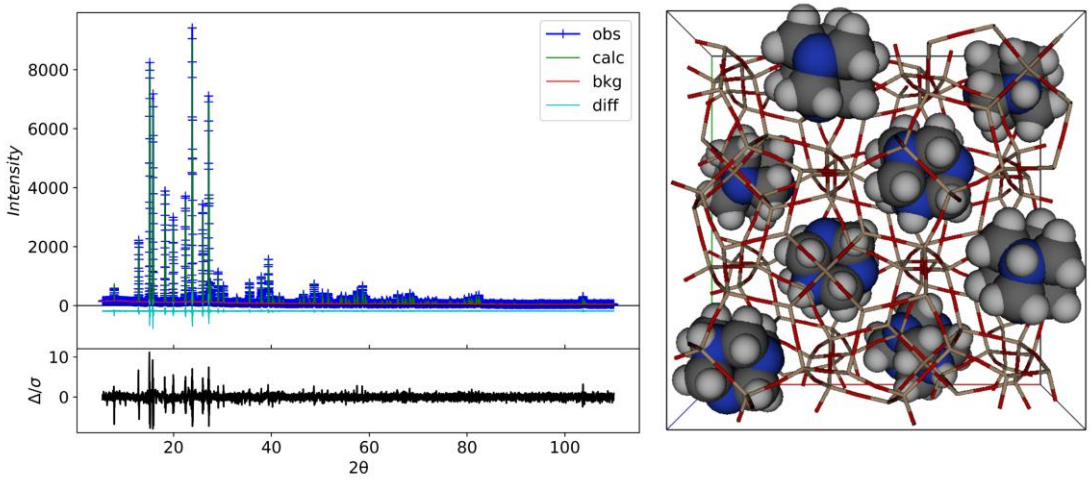

Figure 6. The Rietveld refined XRD pattern fits the experimental (Sample A3), and the refined unit cell with an edge length a=19.39662 Å.

The simulated unit cell model has been validated against experimental XRD (Sample A3), through Rietveld refinement. The crystallographic and experimental parameters are given in Table 2. Refined variables include the instrumental, the histogram profile parameters, and the unit cell length. The atomic coordinates were kept not refined to avoid irrational relaxations in the P1 cell containing 592 atoms. The refinement converged at satisfactory residuals: R_w= 6.862%, reduced χ^2 = 0.650. The fitting of the modelled to the experimental XRD is in Figure 6. It shows that the main mismatches are the peak asymmetry, because the experimental data have been collected in the theta-theta geometry. The mismatches are within a tolerable scale of ca. ±0.1% in peak heights. The refined model, with a new unit cell edge length (a = 19.39662 Å) is illustrated in Figure 6 as well. The refinement parameters and the Crystallographic Information File (MTN_HMTAion.cif) is detailed in the Supplementary Information, in addition to the atomic coordinates in Table S2.1.

The Rietveld refinement has validated the model with $HMTA^+$ ions filling the hexakaidecahedral [$5^{12}6^4$] cages. The $HMTA^+$ cations are located in the cage centers with random orientations at the full occupancy. The model used does not contain F^- ions. This treatment is justified because limited numbers of F^- ions at disordered positions contribute negligibly to the reflections. The model does not consider other local discrepancies, such as the 2% Si defects and the F_x-Si(-OSi)$_3$ bonds, either. The refined model of the long-range crystalline structure can tolerate such structures with random distributions at insignificant concentrations.

In the refined model, all methylene H atoms of $HMTA^+$ have even distances to the nearest framework O atoms, at 3.1±0.2 Å. The host [$5^{12}6^4$] cage and the guest $HMTA^+$ ion perfectly fit each other's shape. In other words, **MTN**'s [$5^{12}6^4$] cage is an exact replica of the $HMTA^+$ cation in shapes. One can scale the power of OSDAs from an unselective space-filler to a selective and tightly fitted "template".[2, 4, 5, 7, 8, 16] In the current case, $HMTA^+$ cation is, therefore, a true template rather than an unselective space-filler for the crystallization of |$HMTA^+$, F^-|-[SiO_2]-dodecasil 3C-**MTN**. This explains the strong structure-directing power of $HMTA^+$, which is not sensitive to water contents in the broad pH range.

Table 2. Crystallographic and experimental (Sample A3) parameters for the Rietveld refinement.

Wavelength (Å)	1.540510/1.544330 (Cu Kα)
Temperature (K)	298
2θ Range (°)	5-120 (5.5-110 used)
Step size (°)	0.01
No. of observations	10451
No. of variables	34
Space group	P1
Unit cell parameters	
a = b= c (Å)	19.39662(0.000194)
α= β= γ (°)	90
Cell volume (Å^3)	7294.230(0.073)
Residuals	
R_{wp}	0.0686
R_p	0.0511
R_F^2	0.0081
Reduced χ^2	0.65

3.4 Complete removal of $HMTA^+$ has not been achieved by calcination in air

Removal of $HMTA^+$ out of **MTN**'s [$5^{12}6^4$] cage to make the void space available for adsorptions of other guest molecules is

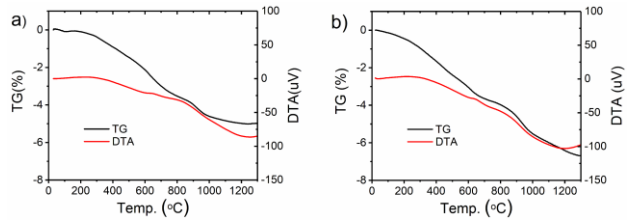

Figure 7. TG/DTA of |HMTA+, F-|-dodecasil 3C-MTN crystallized at a) pH = 6.1 (Sample A3) and b) pH = 4.4 (Sample A6).

challenging because of the small window sizes. Figure 7 depicts the TG/DTA results of the crystals obtained at pH = 6.1 (Sample A3) and pH = 4.4 (Sample A6). The weight content of $HMTA^+$ in the material is calculated at 12.1%. However, upon heating to 1300°C in air the samples lose only 5.2 and 6.6% of weight, respectively. Oxygen molecule can not penetrate the 6-ring window and approach $HMTA^+$. A combustion of the organic ion does not occur. Observable is thermal cracking and leaving of some of the cracking products, which is an uncontrolled process. Therefore the weight losses of the two experiments are different. Recognizable decomposition temperatures of $HMTA^+$ are 590°C with a weak endothermic DTA peak, and 920°C, without a significant heat signal. The samples are black after the TG/DTA tests because of the remaining carbonaceous species. On the other hand, the stability of **MTN** framework structure is extremely good; it does not collapse up to 1300°C in air.

4 Conclusions

This is a sound example of how extending the zeolite synthesis to an acidic medium could be used to provide a structure-directing power in the zeolite synthesis of an organic molecule. Hexamethylene-tetramine (urotropine), with its C/N ratio = 1.5 and high hydrophilicity, does not show a structure-directing ability in the synthesis of zeolites in the basic medium. The protonation of the molecule in an acidic or close to acidic medium converted it into an efficient OSDA generating the **MTN**-type framework in a wide range of synthesis conditions. Experimental details elaborate that dodecasil 3C-**MTN** crystallizes in the presence of protonated urotropine ($HMTA^+$) and NH_4F/HF at pH = 4.4-6.8 in a broad range of water dilution. The protonation of HMTA molecule to cation has altered its affinity to water and silicate species, enabled their exchange in the cation's hydrate shield, and light-off the zeolite crystallization. This approach could be extended to other organic molecules with size and spatial organization appropriate for the generation of zeolite-type materials.

The energy minimization simulation in the force field indicates that the protonated $HMTA^+$ cation resides in the big hexakaidecahedral $[5^{12}6^4]$ cage of **MTN** at the full occupancy. $HMTA^+$ has an approximately spherical shape, is located in the cage center with random orientations, and keeps even distances to the cage walls. Rietveld refinement has been employed to validate the model. The $[5^{12}6^4]$ cage is a replica of $HMTA^+$ regarding the shapes, therefore, the cation has strong directing power for **MTN**-type structure.

Author Contributions

G. Fu: Investigation, Methodology, Writing – original draft. **E. Dib**: Conceptualization, Methodology, Investigation, Writing – review & editing. **Q. Lang, H. Zhao, S. Wang, R. Ding**: Investigation. **X. Yang**: Conceptualization, Methodology, Investigation, Writing – original draft. **V. Valtchev**: Conceptualization, Supervision, Writing – review & editing, Funding acquisition.

Conflicts of interest

There are no conflicts to declare.

Acknowledgements

The ZeoMat Group acknowledges the starting grant provided by QIBEBT, and the support by Shandong Energy Institute (SEI S202107). V.V. and X.Y. acknowledge the collaboration in the framework of the Sino-French International Research Network "Zeolites".

References

1. M. A. Camblor, L. A. Villaescusa and M. J. Díaz-Cabañas, *Topics in Catalysis*, 1999, **9**, 59-76.
2. L. Gómez-Hortigüela and M. Á. Camblor, in *Insights into the Chemistry of Organic Structure-Directing Agents in the Synthesis of Zeolitic Materials*, ed. L. Gómez-Hortigüela, Springer International Publishing, Cham, 2018, DOI: https://doi.org/10.1007/430_2017_8, pp. 1-41.
3. B. M. Lok, T. R. Cannan and C. A. Messina, *Zeolites*, 1983, **3**, 282-291.
4. R. M. Shayib, N. C. George, R. Seshadri, A. W. Burton, S. I. Zones and B. F. Chmelka, *Journal of the American Chemical Society*, 2011, **133**, 18728-18741.
5. A. W. Burton, S. I. Zones and S. Elomari, *Current Opinion in Colloid & Interface Science*, 2005, **10**, 211-219.
6. H. Gies and B. Marker, *Zeolites*, 1992, **12**, 42-49.
7. M. E. Davis, *Nature*, 2002, **417**, 813-821.
8. M. Moliner, F. Rey and A. Corma, *Angewandte Chemie International Edition*, 2013, **52**, 13880-13889.
9. J. Li, A. Corma and J. Yu, *Chemical Society Reviews*, 2015, **44**, 7112-7127.
10. M.-J. Díaz-Cabañas, P. A. Barrett and M. A. Camblor, *Chemical Communications*, 1998, DOI: 10.1039/a804800b, 1881-1882.
11. S. L. Burkett and M. E. Davis, *The Journal of Physical Chemistry*, 1994, **98**, 4647-4653.
12. S. L. Burkett and M. E. Davis, *Chemistry of Materials*, 1995, **7**, 920-928.
13. G. Melinte, V. Georgieva, M.-A. Springuel-Huet, A. Nossov, O. Ersen, F. Guenneau, A. Gedeon, A. Palcic, K. N. Bozhilov, P.-H. Cuong, S. Qiu, S. Mintova and V. Valtchev, *Chemistry-a European Journal*, 2015, **21**, 18316-18327.
14. K. N. Bozhilov, T. T. Le, Z. Qin, T. Terlier, A. Palčić, J. D. Rimer and V. Valtchev, *Science Advances*, 2021, **7**, eabg0454.
15. E. E. Freeman, J. J. Neeway, R. K. Motkuri, J. D. Rimer and G. Mpourmpakis, *AIChE Journal*, 2020, **66**, e17107.
16. R. F. Lobo, S. I. Zones and M. E. Davis, *Journal of inclusion phenomena and molecular recognition in chemistry*, 1995, **21**, 47-78.
17. Y. Kubota, M. M. Helmkamp, S. I. Zones and M. E. Davis, *Microporous Materials*, 1996, **6**, 213-229.
18. P. Wagner, Y. Nakagawa, G. S. Lee, M. E. Davis, S. Elomari, R. C. Medrud and S. I. Zones, *Journal of the American Chemical Society*, 2000, **122**, 263-273.
19. S. I. Zones, A. W. Burton, G. S. Lee and M. M. Olmstead, *Journal of the American Chemical Society*, 2007, **129**, 9066-9079.

20. D. Schwalbe-Koda, S. Kwon, C. Paris, E. Bello-Jurado, Z. Jensen, E. Olivetti, T. Willhammar, A. Corma, Y. Román-Leshkov, M. Moliner and R. Gómez-Bombarelli, *Science*, 2021, **374**, 308-315.
21. D. Shi, K.-G. Haw, C. Kouvatas, L. Tang, Y. Zhang, Q. Fang, S. Qiu and V. Valtchev, *Angewandte Chemie-International Edition*, 2020, **59**, 19576-19581.
22. X. Yang, E. Dib, Q. Lang, H. Guo, G. Fu, J. Wang, Q. Yi, H. Zhao and V. Valtchev, *Microporous and Mesoporous Materials*, 2022, **329**, 111537.
23. H. Zhao, Q. Lang, G. Fu, R. Ding, S. Wang, X. Yang and V. Valtchev, *Microporous and Mesoporous Materials*, 2022, **333**, 111728.
24. D. Zhao, S. Qiu and W. Pang, in *Proceedings from the Ninth International Zeolite Conference*, eds. R. von Ballmoos, J. B. Higgins and M. M. J. Treacy, Butterworth-Heinemann, 1993, DOI: https://doi.org/10.1016/B978-1-4832-8383-8.50039-8, pp. 337-344.
25. C. Baerlocher, L. B. McCusker and D. H. Olson, *Journal*.
26. A. Le Bail, H. Duroy and J. L. Fourquet, *Materials Research Bulletin*, 1988, **23**, 447-452.
27. X. Yang, M. A. Camblor, Y. Lee, H. Liu and D. H. Olson, *J Am Chem Soc*, 2004, **126**, 10403-10409.
28. A. Turrina and P. A. Cox, in *Insights into the Chemistry of Organic Structure-Directing Agents in the Synthesis of Zeolitic Materials*, ed. L. Gómez-Hortigüela, Springer International Publishing, Cham, 2018, DOI: 10.1007/430_2017_16, pp. 75-102.
29. B. H. Toby and R. B. Von Dreele, *Journal of Applied Crystallography*, 2013, **46**, 544-549.
30. H. Rietveld, *Journal of Applied Crystallography*, 1969, **2**, 65-71.
31. H. Gies, F. Liebau and H. Gerke, *Angewandte Chemie International Edition in English*, 1982, **21**, 206-207.
32. J. L. Schlenker, F. G. Dwyer, E. E. Jenkins, W. J. Rohrbaugh, G. T. Kokotailo and W. M. Meier, *Nature*, 1981, **294**, 340-342.
33. D. M. Bibby and L. M. Parker, *Zeolites*, 1983, **3**, 11-12.
34. H. Gies, *Journal of inclusion phenomena*, 1986, **4**, 85-91.
35. Y. Long, H. He, P. Zheng, G. Wu and B. Wang, *Journal of inclusion phenomena*, 1987, **5**, 355-362.
36. J. J. Carroll, in *Natural Gas Hydrates (Second Edition)*, ed. J. J. Carroll, Gulf Professional Publishing, Burlington, 2009, DOI: https://doi.org/10.1016/B978-0-7506-8490-3.00002-1, pp. 17-50.
37. P. Roose, K. Eller, E. Henkes, R. Rossbacher and H. Höke, in *Ullmann's Encyclopedia of Industrial Chemistry*, DOI: https://doi.org/10.1002/14356007.a02_001.pub2, pp. 1-55.
38. H. Tada, *Journal of the American Chemical Society*, 1960, **82**, 255-263.
39. A. P. Cooney, M. R. Crampton and P. Golding, *Journal of the Chemical Society, Perkin Transactions 2*, 1986, DOI: 10.1039/P29860000835, 835-839.
40. H. Strobl, C. A. Fyfe, G. T. Kokotailo, C. T. Pasztor and D. M. Bibby, *Journal of the American Chemical Society*, 1987, **109**, 4733-4734.
41. E. J. J. Groenen, N. C. M. Alma, J. Dorrepaal, G. R. Hays and A. G. T. G. Kortbeek, *Zeolites*, 1985, **5**, 361-363.
42. C. A. Fyfe, H. Gies and Y. Feng, *Journal of the American Chemical Society*, 1989, **111**, 7702-7707.
43. P. Caullet, J.-L. Paillaud, A. Simon-Masseron, M. Soulard and J. Patarin, *Comptes Rendus Chimie*, 2005, **8**, 245-266.
44. E. Dib, J. Grand, S. Mintova and C. Fernandez, *Chemistry of Materials*, 2015, **27**, 7577-7579.
45. C. A. Fyfe, D. H. Brouwer, A. R. Lewis and J.-M. Chézeau, *Journal of the American Chemical Society*, 2001, **123**, 6882-6891.
46. H. Koller, A. Wölker, L. A. Villaescusa, M. J. Díaz-Cabañas, S. Valencia and M. A. Camblor, *Journal of the American Chemical Society*, 1999, **121**, 3368-3376.
47. Z. S. Lin, D. Chen, H.-Y. Nie, Y. T. A. Wong and Y. Huang, *Canadian Journal of Chemistry*, 2019, **97**, 840-847.
48. T. Shimizu, M. Kumeda, H. Komatsu and Y. Yonezawa, *Journal of Non-Crystalline Solids*, 1985, **77-78**, 719-722.